Transportation Research Part B 93 (2016) 560–575

Contents lists available at ScienceDirect

Transportation Research Part B

journal homepage: www.elsevier.com/locate/trb

Cellular automaton model simulating spatiotemporal patterns, phase transitions and concave growth pattern of oscillations in traffic flow

Junfang Tian[a], Guangyu Li[a,*], Martin Treiber[c], Rui Jiang[b,*], Ning Jia[a], Shoufeng Ma[a]

[a] Institute of Systems Engineering, College of Management and Economics, Tianjin University, Tianjin 300072, China
[b] MOE Key Laboratory for Urban Transportation Complex Systems Theory and Technology, Beijing Jiaotong University, Beijing 100044, China
[c] Technische Universität Dresden, Institute for Transport & Economics, Würzburger Str. 35, D-01062 Dresden, Germany

ARTICLE INFO

Article history:
Received 2 July 2015
Revised 14 August 2016
Accepted 22 August 2016

Keywords:
Three-phase traffic theory
Traffic oscillations
Cellular automaton

ABSTRACT

This paper firstly shows that a recent model (Tian et al., Transpn. Res. B 71, 138–157, 2015) is not able to replicate well the concave growth pattern of traffic oscillations (i.e., the standard deviation of speed is a concave function of the vehicle number in the platoon) observed from car following experiments. We propose an improved model by introducing a safe speed and the logistic function for the randomization probability. Simulations show that the improved model can reproduce well the metastable state, the spatiotemporal patterns, and the phase transitions of traffic flow. Calibration and validation results show that the concave growth pattern of oscillations and the empirical detector data can be simulated with a quantitative agreement.

1. Introduction

The formation and evolution of traffic congestion has been investigated for decades (see e.g., Brackstone and McDonald, 1999; Chowdhury et al., 2000; Helbing, 2001; Nagatani, 2002; Treiber and Kesting, 2013; Kerner, 2004, 2009, 2013, 2016; Saifuzzaman and Zheng, 2014; Zheng, 2014; Jin et al., 2015). Various traffic flow data have been collected to clarify the nature of traffic flow dynamics (Ranjitkar et al., 2003; Kerner, 2004; Bertini and Monica, 2005; NGSIM, 2006; Laval and Daganzo, 2006; Ahn and Cassidy, 2007; Wagner, 2006, 2010, 2012; Sugiyama et al., 2008; Nakayama et al., 2009; Zheng et al. 2011; Shott, 2011; Tadaki et al., 2013; Laval et al., 2014; Jiang et al. 2014, 2015). In order to simulate traffic flow, different kinds of models have been proposed, such as the car-following models (Chandler et al. 1958; Newell, 2002; Rakha and Crowther, 2003; Kesting and Treiber, 2008; Laval and Leclercq, 2010;Chen et al. 2012a, 2012b; Aghabayk et al. 2013; He et al. 2015), the cellular automata models (Nagel and Schreckenberg, 1992; Knospe et al., 2000; Kerner et al., 2002, B.S. 2011) and hydrodynamic models (Lighthill and Whitham, 1955; Papageorgiou 1998; Wong and Wong 2002).

Many traditional models, such as the General Motor models (GMs, Chandler et al., 1958; Gazis et al. 1961; Edie, 1961), Gipps' Model (Gipps, 1981), Optimal Velocity Model (OVM, Bando et al., 1995), Full Velocity Difference Model (FVDM, Jiang et al., 2001), Intelligent Driver Model (IDM, Treiber et al., 2000) and so on, are classified as two-phase models

* Corresponding authors.
E-mail addresses: jftian@tju.edu.cn (J. Tian), liguangyuli@hotmail.com (G. Li), jiangrui@bjtu.edu.cn (R. Jiang).

http://dx.doi.org/10.1016/j.trb.2016.08.008
0191-2615/

(Kerner, 2013). In two-phase models, only free flow (F) and congested flow states are distinguished, and the formation of traffic jams is explained via linear instability.

However, by analyzing the long-term detector data, Kerner (1998) further distinguished congested traffic into wide moving jams (J) and synchronized traffic flow (S). The wide moving jam is a moving structure in which vehicles stop completely or nearly. The downstream front of a jam moves upstream with a characteristic speed about 15 km/h. In contrast, synchronized flow is usually fixed at traffic bottlenecks and the flow rate in the synchronized flow is much larger than that in jam. For the synchronized flow that moves upstream, the propagating speed of its downstream front is not necessarily the characteristic speed. Based on these observations, Kerner proposed the three-phase traffic theory, in which it is hypothesized that the steady states of synchronized flow should cover a two-dimensional region in the flow–density plane. Based on Kerner's three-phase traffic theory, many models have been developed, such as the Kerner-Klenov-Wolf model (KKW, Kerner et al., 2002) that considers the speed adaptation effect, the model that considers mechanical restriction versus human overreaction (Lee et al., 2004), the Brake Light Model (BLM, Knospe et al., 2000) and its variants (Jiang and Wu, 2003, 2005; Tian et al., 2014, 2016b) that consider the influence of brake light on driving behaviors, the model that assumes that randomization depends on speed difference (the model of Gao, Gao et al. 2007, K. 2009), and so on. These models have been claimed to be able to simulate the observed spatiotemporal patterns of traffic flow.

Kerner (2004, 2009, 2013, 2016) claimed that traffic breakdown corresponds to a phase transition from free flow to synchronized flow (F→S) while wide moving jams usually emerge from the synchronized flow (S→J). As a result, the transition from free flow to jams corresponds to a F→S→J process. In an open road section with an isolated bottleneck, two types of spatiotemporal traffic patterns can be observed: the general pattern (GP) and the synchronized pattern (SP). In SP, no traffic jam occurs. In contrast, in GP, jams will eventually develop in the synchronized flow. The associated self-compression effect that initiates jams is named as pinch effect and this self-compression of synchronized flow means that the average density increases and average speed decreases considerably in the synchronized flow (Kerner, 2009).

Spontaneous formations of jams have been observed in the absence of any bottleneck as well. For example, Treiterer and Myers (1974) have shown the trajectories of a phantom jam. Coifman (1997) also presented the trajectories of thirteen shockwaves in platoons, where a small disturbance grows as it propagates upstream until vehicles come to a stop. Sugiyama et al. (2008), Nakayama et al. (2009), and Tadaki et al. (2013) performed traffic experiments on a circuit to investigate the emergence of a jam without bottleneck. The experiments showed that when the density is below a critical value, traffic flow is unconditionally stable and no jam emerges. However, above another critical density, traffic flow always becomes unstable and jam always occurs spontaneously. Between the two critical densities, traffic flow is metastable and the spontaneous formation of jam can be observed probabilistically.

Recently, Tian et al. (2015) have proposed a Two-state cellular automaton model to simulate these empirical features, in which the defensive state and the normal state of drivers have been considered. In the Two-state model, the space gap between two vehicles will oscillate around the (speed dependent) desired value rather than maintaining this value in the deterministic limit in congested traffic flow. It was shown that the model is able to simulate above-mentioned spatiotemporal patterns and phase transitions very well.

In the meantime, however, another important feature of traffic flow concerning the propagation of oscillations in platoons has been reported. Jiang et al. (2014, 2015) carried out a car following experiment on a 3.2 km-long open road section, in which a platoon of 25 passenger cars has been studied. The leading vehicle was asked to move with constant speed. The formation and development of oscillations have been observed. It has been found that standard deviations of speed increase in a concave or linear way along the 25-car-platoon. For the latter case, due to the physical limits of speeds, unconditional concavity, i.e., a decreasing increment of the amplitude from car to car is expected for sufficiently large platoons. Later, the concave growth pattern of oscillations is also validated by the empirical NGSIM data (Tian, et al., 2016a).

Moreover, Jiang et al. (2014, 2015) have shown that (i) the simulation results of the two-phase models with additional reasonable acceleration noise, such as GMs, Gipps' Model, OVM, FVDM and IDM etc., run against the experimental finding since the standard deviation initially increases in a convex way in the unstable density range; (ii) by removing the fundamental diagram in two-phase models and allowing the traffic state to span a two-dimensional region in velocity-spacing plane, the growth pattern of disturbances has changed and becomes qualitatively in accordance with the observations. In particular, the two-dimensional Intelligent Driver Model (2D-IDM) considering variable desired time headway can fit the experimental results quantitatively well.

The importance of the concave growth of traffic oscillations lies in that it indicates that the instability mechanism of traditional two-phase models is debatable. In traditional models, the unstable traffic flow is generated due to linear instability of the steady state solution. As proved by Li et al. (2014), the linear instability in a class of car-following models leads to initial convex growth of oscillations. We further demonstrate that the linear instability in general two-phase models leads to initial convex growth of oscillations (Tian et al., 2016a). Thus, the initial convex growth pattern in Two-phase models contradicts with the observed concave growth pattern, which implies that the mechanism triggering traffic jams in two-phase models is questionable.

Motivated by the new experimental finding, we examine whether the Two-state model is able to reproduce the concave growth pattern of oscillations or not. Unfortunately, as shown in Section 2.1, simulation results of the two-state model significantly deviate from the experimental data. To overcome the deficiency of the two-state model, this paper proposes an improved model which is simultaneously able to reproduce the spatiotemporal patterns, the phase transitions, and the concave growth pattern of oscillations.

Table 1
Parameter values of Two-state model.

Parameters	L_{cell}	L_{veh}	v_{max}	T	p_a	p_b	p_c	a	$b_{defense}$	g_{safety}	t_c
Units	M	L_{cell}	L_{cell}/s	s	–	–	–	L_{cell}/s^2	L_{cell}/s^2	L_{cell}	s
Value	7.5	1	5	1.8	0.95	0.55	0.1	1	1	2	8

The paper is organized as follows. Section 2.1 reviews the original Two-state model and shows its deficiency. Section 2.2 analyzes the Two-state model with refined cell length 0.5 m. Section 2.3 presents the improved Two-state model. Section 3 carries out simulations with the improved model and shows that it can reproduce well the spatiotemporal patterns and the phase transition behavior in traffic flow. Section 4 tests the performance of the improved model and demonstrates that concave growth pattern of oscillations and the empirical detector data can be quantitatively reproduced. Section 5 concludes the paper.

2. The Two-state safe-speed model

2.1. Two-state model

For consistency of the paper, let us briefly review the Two-state model. The update rules of Two-state model are:

1. Deterministic speed update (for a time step $\Delta t = 1$ s):

$$v'_{det} = \min(v + a, v_{max}, d_{anti})$$

2. Stochastic deceleration:

$$v' = \begin{cases} \max(v'_{det} - b_{rand}, 0) & \text{with probability } p \\ v'_{det} & \text{otherwise} \end{cases}$$

3. Determination of stop time tst:

$$t_{st} = \begin{cases} t_{st} + 1 & \text{if } v = 0 \\ 0 & \text{otherwise} \end{cases}$$

4. Position update:

$$x' = x + v'$$

Here v (v') and x (x') are the speeds and positions at the actual and next time step, respectively. $d_{anti} = d + \max(v_{anti} - g_{safety}, 0)$ is the anticipated space gap. $d = x_l - x - L_{veh}$ is the real space gap, L_{veh} is the vehicle length and x_l is the position of the leading vehicle. $v_{anti} = \min(d_l, v_l + a, v_{max})$ is the expected speed of the preceding vehicle in the next time step. g_{safety} is a safety parameter to avoid accidents and the constraint $g_{safety} \geq b_{rand}$ should be satisfied. The anticipated gap was introduced since when a car is moving, its preceding car also probably moves. Therefore, a car can move beyond the limit of real gap. a is the maximum acceleration. The randomization probability p and randomization deceleration b_{rand} are defined as:

$$p = \begin{cases} p_b & \text{if } v = 0 \text{ and } t_{st} > t_c \\ p_c & \text{else if } v \leq d_{anti}/T \\ p_a & \text{otherwise} \end{cases} \quad (1)$$

$$b_{rand} = \begin{cases} a & \text{if } v \leq d_{anti}/T \\ b_{defense} & \text{otherwise} \end{cases} \quad (2)$$

where T is the effective safe time gap. t_{st} denotes the stopped time of vehicles. The Two-state model has considered two driver states: a defensive one, and a normal one. The defensive state is activated if $v > d_{anti}/T$. Otherwise the drivers are assumed to be in the normal driving state.

The parameter values of the Two-state model are shown in Table 1. Fig. 1 presents simulation results of car following process of a 25-car-platoon (see Section 4.1 for details of the simulation setup). Since the cell length is set to $L_{cell} = 7.5$ m, the Two-state model cannot describe the detailed structure of traffic flow. Specifically, the velocities of the cars in the platoon can only be equal to 27 km/h ($1L_{cell}/s$), 54 km/h ($2L_{cell}/s$), 81 km/h ($3L_{cell}/s$), and so on. As a result, one can only make a rough comparison between simulation and experiment. Fig. 1 shows that even a rough comparison demonstrates that the standard deviation deviates significantly from the experimental data. Moreover, the spatiotemporal characteristics are not consistent with the experimental one, either.

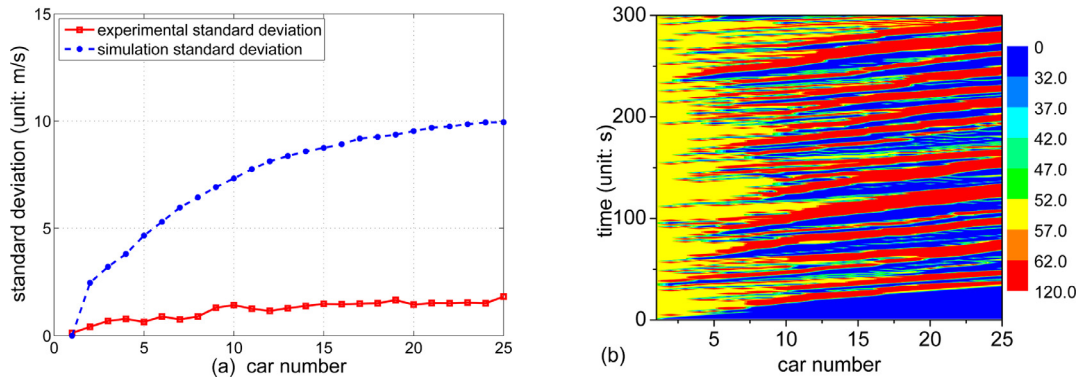

Fig. 1. (a) Comparison of the simulation result and experiment result of the standard deviation of the velocities of the cars and (b) the spatiotemporal patterns of the platoon traffic when the leading vehicle moves with the constant speed $v_{leading} = 54$ km/h. The color bar in (b) indicates speed. In the real experiment, the leading vehicle is required to move with $v_{leading} = 50$ km/h.

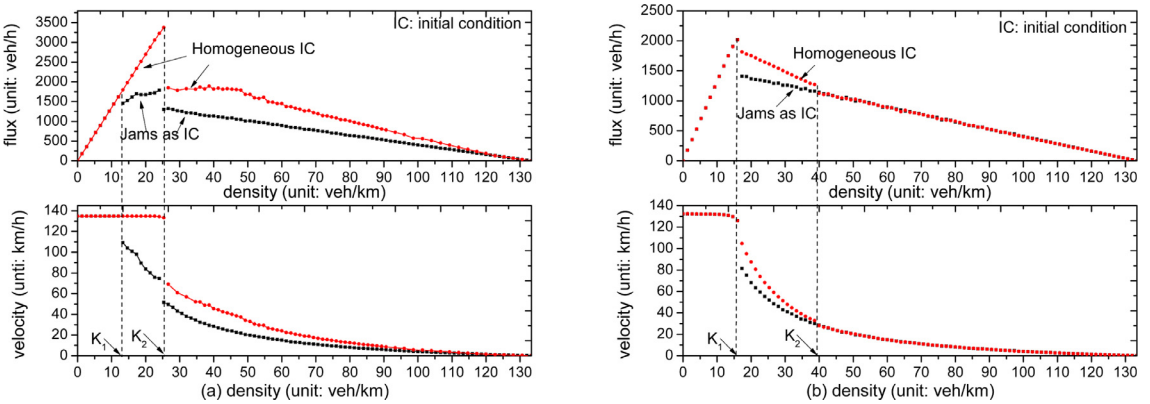

Fig. 2. Flow-density and speed-density diagrams of (a) Two-state model with $L_{cell} = 0.5$ m and (b) Two-state model with default $L_{cell} = 7.5$ m. "Homogeneous IC" represents the initially homogeneous distribution of traffic, and "Jams as IC" represents the initially mega-jam distribution of traffic.

Table 2
Parameter values of Two-state model with refined cell length.

Parameters	L_{cell}	L_{veh}	v_{max}	T	p_a	p_b	p_c	a	$b_{defense}$	g_{safety}	t_c
Units	M	L_{cell}	L_{cell}/s	s	–	–	–	L_{cell}/s^2	L_{cell}/s^2	L_{cell}	s
Value	0.5	15	75	1.8	0.95	0.55	0.1	1	1	2	8

2.2. Two-state model with refined cell length

To better describe the detailed structure of traffic flow, we set the cell length $L_{cell} = 0.5$ m, and parameter values are shown in Table 2. Fig. 2(a) shows the flow-density and speed-density diagrams of the model with the refined cell length (see Section 3.1 for details of the simulation setup). As a comparison, the results of the Two-state model with $L_{cell} = 7.5$ m are presented in Fig. 2(b), which shows that the flow-density and speed-density diagrams are significantly different from that with $L_{cell} = 0.5$ m. The homogeneous initial condition results in the coexistence state of synchronized flow and free flow in the Two-state model with $L_{cell} = 7.5$ m (Fig. 3(a)), however, it leads to a strange state when reducing the cell length to $L_{cell} = 0.5$ m (Fig. 4(a)). For the mega-jam initial condition, both models show the coexistence of wide moving jams and free flow (Fig. 3(b) and Fig. 4(b)). However, in the density range $K > K_1$, traffic flow initiated from the homogeneous initial condition is always stable, and its flux and speed are higher than that from the mega-jam initial condition. This is also inconsistent with that of the Two-state model with $L_{cell} = 7.5$ m and not in line with reality since wide moving jams will emerge finally in the high density region.

2.3. Two-state safe-speed model

In the Two-state model, there exist intrinsic large fluctuations. In order to make the model more realistic, we introduce the safe speed v_{safe} (defined by the simplified Gipps model (see Equation 11.10 of Treiber and Kesting, 2013)), and the

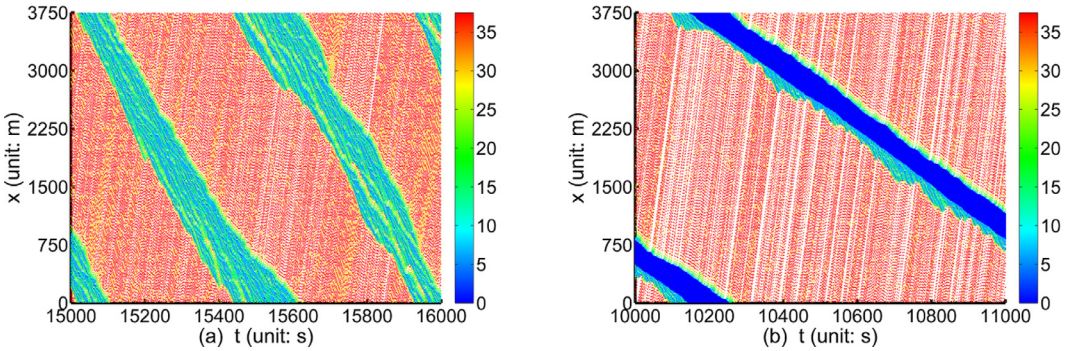

Fig. 3. The spatiotemporal diagrams of Two-state model with $L_{cell} = 7.5$ m on the circular road with the density $k = 24$ veh/km. In (a) the traffic starts from a homogenous initial distribution. In (b) the traffic starts from a megajam. The horizontal direction (from left to right) is time and the vertical direction (from down to up) is space. The color bar indicates speed. (For interpretation of the references to colour in this figure legend, the reader is referred to the web version of this article.)

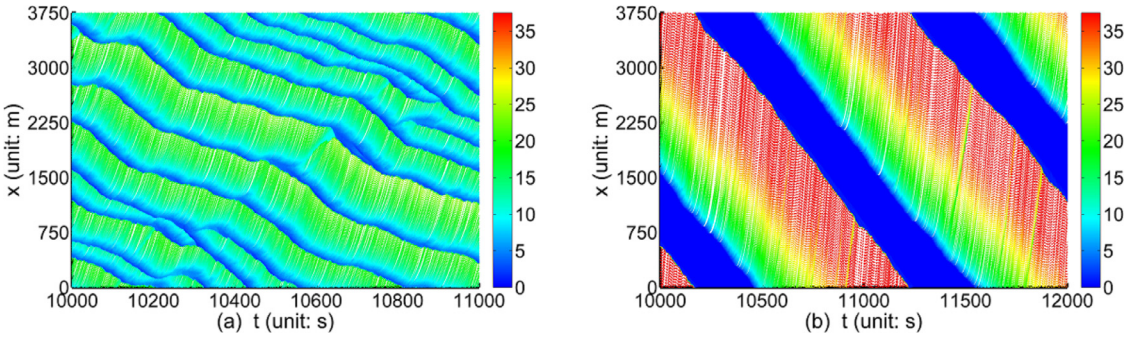

Fig. 4. The spatiotemporal diagrams of Two-state model with $L_{cell} = 0.5$ m on the circular road with the density $k = 48$ veh/km. In (a) the traffic starts from a homogeneous initial distribution. In (b) the traffic starts from a megajam. The color bar indicates speed. (For interpretation of the references to colour in this figure legend, the reader is referred to the web version of this article.)

logistic function for the randomization probability p_{defense} into the Two-state model to avoid large decelerations and large fluctuations. The two new variables are defined as follows:

$$v_{\text{safe}} = \left[-b_{\max} + \sqrt{b_{\max}^2 + v_l^2 + 2b_{\max}d}\right] \tag{3}$$

$$p_{\text{defense}} = p_c + \frac{p_a}{1 + e^{\alpha(v_c - v)}} \tag{4}$$

where α and v_c are the steepness and midpoint of the logistic function, respectively. The round function $[x]$ returns the integer nearest to x.

The safe speed v_{safe} is applied to take into consideration kinematic restraints restricting the maximum safe speed of a vehicle when its space gap is d and the preceding car moves with v_l. It is calculated based on the assumption that (i) the driver's reaction time is equal to one time step, i.e., 1 s; (ii) the maximum deceleration of the vehicle is $b_{\max}$; (iii) the preceding car decelerates with $b_{\max}$ and the deceleration of the considered vehicle is restricted to $b_{\max}$ as well. Note that Eq.(4) heuristically defines pdefense as a function of the speed based on the observations. Fig. 5 illustrates the shape for the randomization probability p_{defense} defined by Eq. (4). It can be seen that when the speed v is lower than v_c, the randomization probability is greatly reduced.

Using the new variables, the Two-state model is improved as follows:

1. Deterministic speed update:

$$v'_{\text{det}} = \min(v + a, v_{\max}, d_{\text{anti}}, v_{\text{safe}})$$

2. Stochastic deceleration:

$$v' = \begin{cases} \max(v'_{\text{det}} - b_{\text{rand}}, 0) & \text{with probability } p \\ v'_{\text{det}} & \text{otherwise} \end{cases}$$

3. Position update:

$$x' = x + v'$$

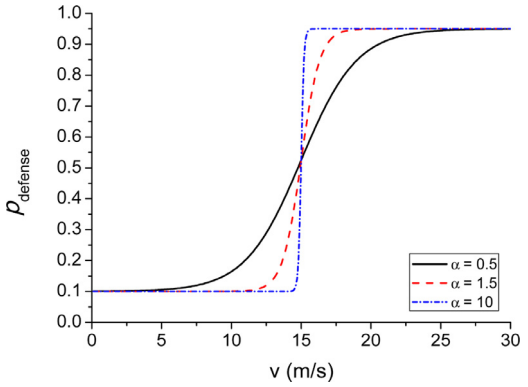

Fig. 5. The logistic form of $p_{defense}$ for $v_c = 15$ m/s, $v_{max} = 30$ m/s, $p_c = 0.1$, and $p_a = 0.85$.

where the randomization deceleration brand is defined by

$$b_{rand} = \begin{cases} a & \text{if } v < b_{defense} + \lfloor d_{anti}/T \rfloor \\ b_{defense} & \text{otherwise} \end{cases} \tag{5}$$

while the randomization probability p is redefined as:

$$p = \begin{cases} p_b & \text{if } v = 0 \\ p_c & \text{else if } v \le d_{anti}/T \\ p_{defense} & \text{otherwise} \end{cases} \tag{6}$$

In Eq. (5), the floor function $\lfloor x \rfloor$ returns the maximum integer no greater than x. Note that Eq. (5) is different from Eq. (2), in which the criterion between the defensive and the normal state has been modified. This modification further suppresses the intrinsic fluctuations at low velocities and thus makes the growth pattern of oscillations at low velocities quantitatively consistent with the experimental data. Due to the introduction of the safe speed, this model is named as the Two-state Safe-speed Model (TSM). Since the fluctuations are greatly reduced and velocity in the synchronized flow will not decrease to zero, Step 3 (i.e. Determination of stop time tst) of Two-state model is removed in TSM.

Compared with the Two-state model, the TSM contains two main additional ingredients: (i) The restriction to a kinematically well-justified safe speed makes sure that, under normal car-following situations, the desired maximum braking deceleration b_{max} is not exceeded, which can reduce the intrinsic fluctuations. (ii) a smaller randomization probability is used at low speeds, which can further reduce the intrinsic fluctuations for low speed vehicles. In the following simulations, we will show that these two ingredients enable the TSM to be closer to reality.

In contrast to the KKW model, the TSM assumes a behavioral change when the anticipated time gap (i.e., d_{anti}/v) is equal or below T rather than an explicit range of indifference for the gaps. Furthermore, the TSM includes a safe speed restricting the braking deceleration in all normal situations.

2.4. Discussion

One might argue that CA models with a small cell size defeat the purpose of the CA paradigm, namely providing simple and numerically efficient models that can be simulated without further assumptions. In fact, compared with car-following models,, the advantages of CA models regarding simulation speed are (i) the update time step is usually set to 1 *s*, which is based on a typical driver's reaction time (Maerivoet, De Moor, 2005; Chowdhury, Santen, Schadschneider, 2000), while the numerical time step is much smaller in car-following models (typically, 0.1 s).[1] (ii) the space is discretized and represented by integers while it is a real number in car-following models.[2] As a result, the simulation speed of CA models is much faster. Although, nowadays, the computer speed is greatly enhanced, the simulation speed remains important, particularly in large-scale microscopic simulations.

Another advantage of CA models is that the update rules are unique and can be directly computed while the integration of the differential equations of time-continuous car-following models depends on the chosen numerical method. We emphasize that the aforementioned numerical advantages of CA models do not depend on cell size and, therefore, decreasing cell size does not defeat the purpose of the CA paradigm. Moreover, the original cell size 7.5 m implies a speed discretization of 27 km/h making it just useless to calculate speed standard deviation curves as that in Fig. 10. Besides, nearly all CA models

[1] Note however, in the Newell (2002) model, the numerical time step is set equal to time delay τ, which is of the order of 1s.

[2] Notice, however, that also CA models entail real-number calculations for everything having to do with stochasticity.

Table 3
Parameter values of TSM.

Parameters	L_{cell}	L_{veh}	v_{max}	T	p_a	p_b	p_c	a	b_{max}	$b_{defense}$	g_{safety}	v_c	α
Units	M	L_{cell}	L_{cell}/s	s	–	–	–	L_{cell}/s^2	L_{cell}/s^2	L_{cell}/s^2	L_{cell}	L_{cell}/s	s/L_{cell}
Value	0.5	15	60	1.8	0.85	0.52	0.1	1	7	2	20	30	10

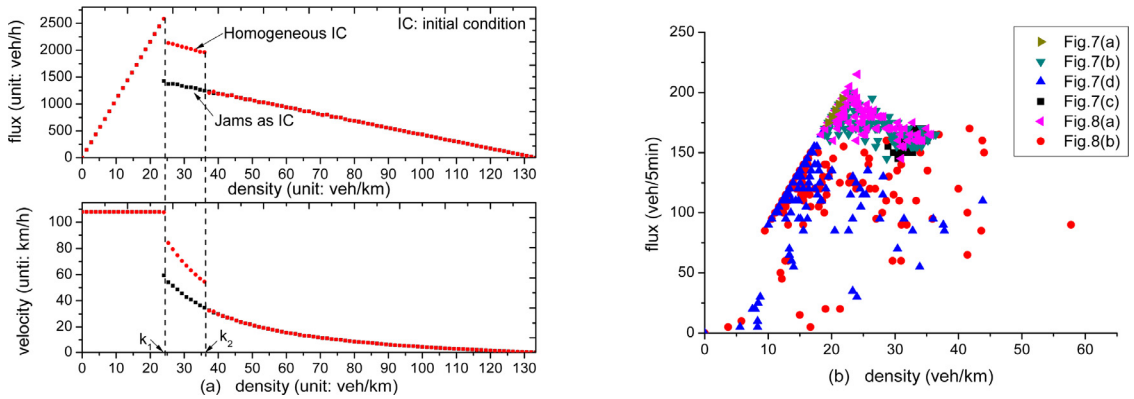

Fig. 6. (a) Flow-density and speed-density diagrams of TSM simulations on a ring road describing the averaged flow (or speed) of traffic flow as a function of the global density. The upper branch between K_1 and K_2 corresponds to a coexistence of free traffic and synchronized flow, while the lower branch at $K > K_1$ corresponds to a coexistence of free traffic and jams. "Homogeneous IC" represents the initially homogenous distribution of traffic, and "Jams as IC" represents the initially mega-jam distribution of traffic. (b) One minute average data corresponding to Panel (a) where the flux J and the arithmetic means of speed $<v>$ are obtained by a virtual detector, and the density ρ is determined via $\rho = J/<v>$.

with the focus on a rather realistic reproduction of the traffic flow dynamics have small cell sizes (starting with the KKW model which has a cell size of 0.5 m as well).

One might also argue that decreasing the cell size could violate stability conditions. Actually numerical stability depends on cell size (or the numerical spatial grid size in case of finite-difference methods) only if the model in question is formulated in the Euler frame of reference (fixed observer) which is the case for most macroscopic models, including the cell-transmission model. Then, the so-called CFL criterion (see Chap. 9.5.5 in Treiber and Kesting, 2013) is violated for too small cell sizes. However, the CFL does not apply for models formulated in the Lagrangian view (moving observer) that is relevant for car-following models and CA models, where, in contrast to the basic CAs, inter-vehicle gaps and vehicle speeds rather than occupation numbers are the primary dynamic variables. Another numerical instability that does apply for both views, regardless of the existence and size of cells, is the “relaxation instability" (see p.152 in Treiber and Kesting, 2013). The relaxation instability becomes active if the update time is larger than the smallest internal dynamic scale controlling the adaptation of gaps and speeds, which is a few seconds in our model. As we mentioned above, the update time step in our proposed model is set to 1 *s*, so there is no relaxation instability for plausible parameter settings.

3. General properties of TSM

This section presents simulation results of the TSM. We investigate traffic flow on a circular road and on an open road with an on-ramp and compare the results with the experimental and empirical findings of Sugiyama et al. (2008), Nakayama et al. (2009), Tadaki et al. (2013), and Kerner (2004, 2009). The cell length L_{cell} and vehicle length L_{veh} are set as 0.5 m and 7.5 m, respectively, i.e. $L_{veh} = 15L_{cell}$. One time step corresponds to 1 *s*. The other parameter values are shown in Table 3.

3.1. Circular road

The following two initial configurations are used in the simulations: 1) all vehicles are homogeneously distributed on the road; 2) all vehicles are distributed in a mega-jam. Fig. 6(a) shows the resulting flow-density and speed-density diagrams, where the upper branch ($K_1 < K < K_2$) is from the initial homogeneous distribution, while the lower branch is from the initial mega-jam ($K_1 < K < K_2$). If the density is smaller than K_1, there is only free flow on the road (Fig. 7(a)). If the density is in the range of $K_1 < K < K_2$, synchronized flow begins to develop from free flow (Fig. 8(a)) and eventually coexists with free flow (Fig. 7(b)). Increasing the density further, free flow will disappear and only synchronized flow can be found (Fig. 7(c)). When the density is greater than K_2, the synchronized flow is unstable, and wide moving jams will appear (Fig. 8(b)), which is similar to the experimental results of Nakayama et al. (2009) (see Fig. 2 in Nakayama et al., 2009). For the lower branch formed from the initial mega-jam, traffic will evolve to the state that wide moving jams and free flow coexist (Fig. 7(d)). Fig. 6(b) shows the one-minute average flux and density, in which the maximum flux and its corresponding density are almost the same as that of the empirical data (see Fig. 1 in Tadaki et al. 2013).

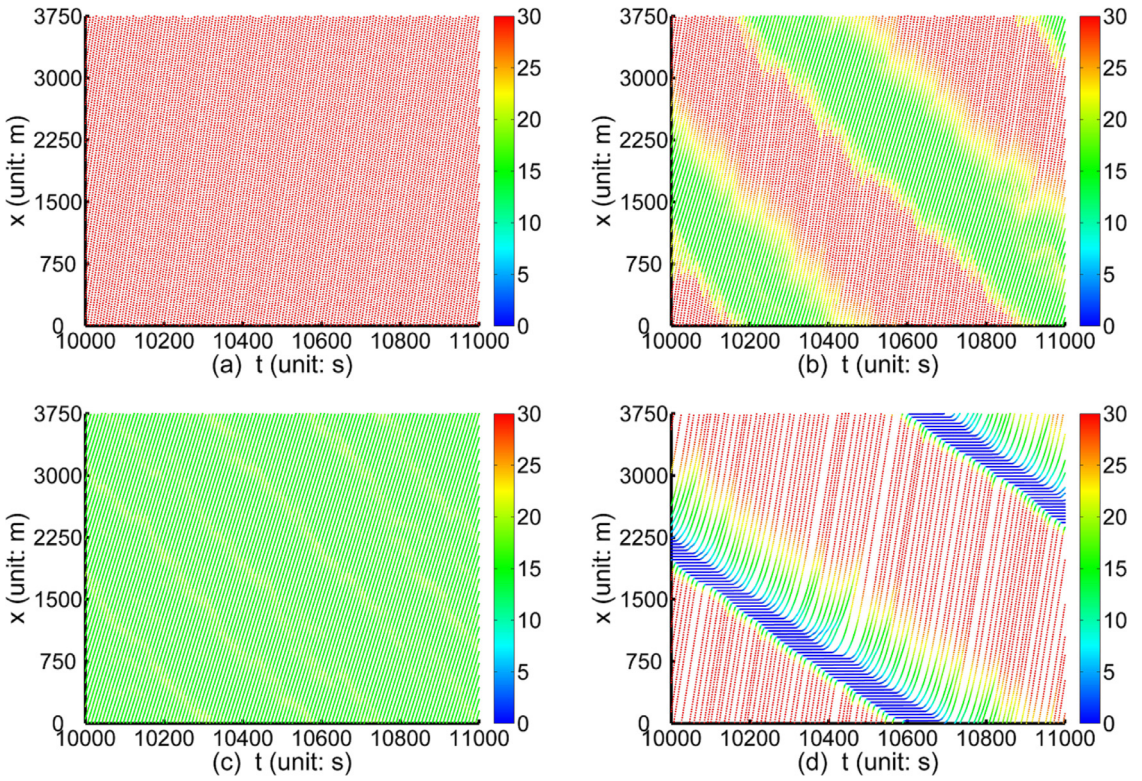

Fig. 7. Spatiotemporal patterns of the TSM on a circular road. In (a-d), the density $k = 21$, 27, 35 and 27 veh/km, respectively. In (a-c), the traffic starts from a homogeneous initial distribution, and in (d) from a mega-jam. The color bar indicates speed. (For interpretation of the references to colour in this figure legend, the reader is referred to the web version of this article.)

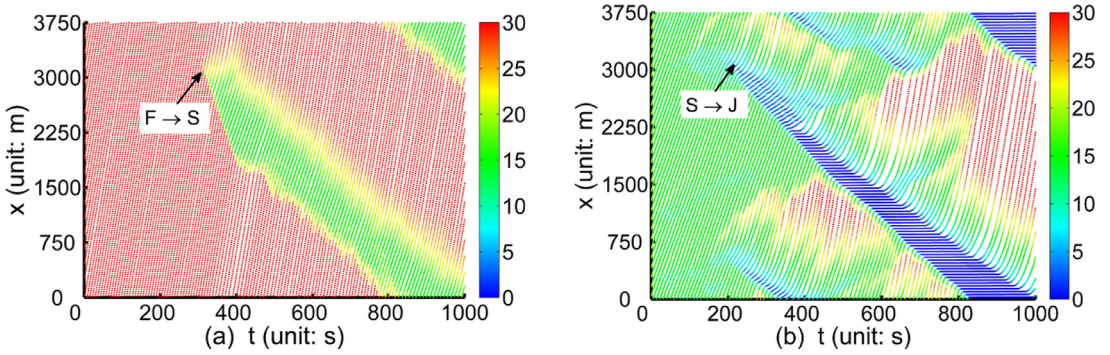

Fig. 8. The F→S and S→J transitions of the TSM on the circular road when starting from a homogenous initial distribution. (a) density $k = 24$ veh/km; (b) $k = 40$ veh/km. The color bar indicates speed. (For interpretation of the references to colour in this figure legend, the reader is referred to the web version of this article.)

3.2. Open road with an on-ramp

Now we study the traffic patterns that emerge near an on-ramp on an open road. Initially, the road section is assumed to be filled with vehicles uniformly distributed with density ρ and all speeds are set to $v_{\max}$. At the downstream boundary, the leading vehicle will be removed once it goes beyond L_{road} and the next car becomes the new leader moving freely until it is taken out as well. At the upstream boundary (road section entrance), no vehicle is inserted. This simulation setup is used because it turned out to be difficult to produce inflows near capacity by inserting cars. Notice that this means that the inflow is defined indirectly by the initial density via the free branch of the flow-density diagram and that the duration of the inflow is restricted by the system size.

In the on-ramp region, a vehicle will be inserted centrally into the biggest gap between two main-road vehicles with the probability $q_{\text{on}}/3600$ once this gap exceeds the critical value $d_{\text{cri}} = \beta L_{\text{veh}} + \gamma v_{\text{l}}$ (where v_{l} is the velocity of the leading vehicle, $\gamma = 0.8$ and $\beta = 1.5$). Here, q_{on} denotes the traffic flow from the on-ramp in vehicles per hour. The length of the on-ramp region is set as $L_{\text{ramp}} = 30 L_{\text{veh.}}$

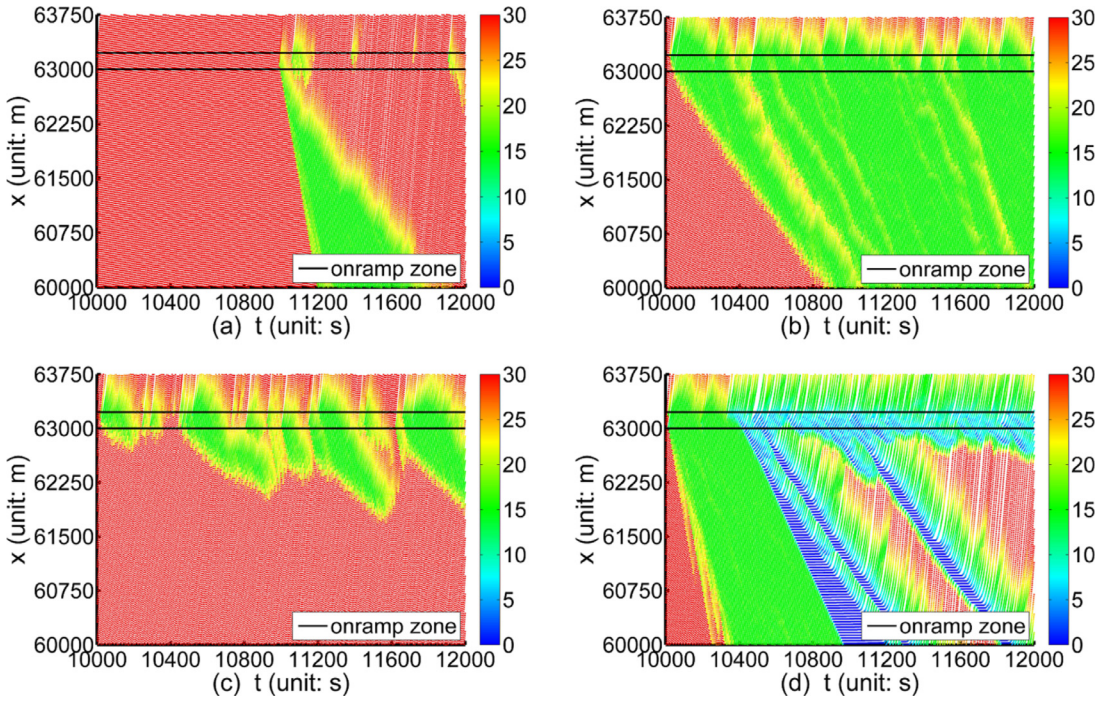

Fig. 9. The spatiotemporal diagrams of TSM on an open road with an on-ramp. (a) MSP: $\rho = 23$ (veh/km), $q_{on} = 9$ (veh/h), (b) WSP: $\rho = 20$ (veh/km), $q_{on} = 49$ (veh/h), (c) LSP: $\rho = 19$ (veh/km), $q_{on} = 54$ (veh/h), (d) GP: $\rho = 22$ (veh/km), $q_{on} = 188$ (veh/h). The color bar indicates speed. (For interpretation of the references to colour in this figure legend, the reader is referred to the web version of this article.)

With this setup, we simulate several spatiotemporal patterns that are also observed in real traffic: Fig. 9(a) shows the moving synchronized flow (MSP, see the empirical example Fig. 7.6 in Kerner (2009)) where both the upstream and downstream fronts propagate along the upstream direction of traffic flow. Fig. 9(b) exhibits the widening synchronized flow (WSP, see the empirical example Fig. 7.4 in Kerner (2009)), where only the upstream front propagates upstream and no wide moving jams appear. Fig. 9(c) gives the local synchronized pattern (LSP, see the empirical example Fig. 7.2 in Kerner (2009)) where the synchronized flow is only localized in the vicinity of the on-ramp region. Finally, Fig. 9(d) shows the general pattern (GP, see the empirical example Fig. 7.9 in Kerner (2009)) where wide moving jams continuously emerge from the synchronized traffic flow upstream of the on-ramp bottleneck. Therefore, the main empirical findings are successfully simulated by the TSM.

Moreover, the propagation velocity of the downstream front of the simulated MSP is about −14 km/h, which falls into the realistic range between −20 and −10 km/h (Treiber, et al. 2010). This is a remarkable characteristic of the TSM, because this velocity is unrealistically negative in most models that could simulate the MSP. For example, in the Two-state and KKW models, the velocity is about −27 km/h and −30 km/h, respectively.

4. Model calibration and validation by traffic data

4.1. Calibration and validation by the experimental data

In this section, we calibrate and validate the TSM by the car-following experimental data of Jiang et al. (2014). In the experiments, the driver of leading vehicle of the platoon was asked to move with the speed $v_{\text{leading}} = 50$, 40, 30, 15, and 7 km/h, respectively. At each v_{leading}, several runs were carried out. The stationary state data have been used to calculate the speed standard deviation, and the results have been averaged over the runs. As shown in Fig. 10, $\sigma_{v,n}$ increases in a concave or linear way along the vehicles n of the platoon.

Next, we use the curves for the standard deviations $\sigma_{v,n}$ under $v_{\text{leading}} = 50$ and 7 km/h to calibrate the TSM and use $\sigma_{v,n}$ under $v_{\text{leading}} = 40$, 30 and 15 km/h for validation. Since the TSM is a cellular automaton model, we cannot make the leading car of the simulated platoon move with exactly the speed of the leading car of the real platoon. Thus, we let the leading vehicle of the simulated platoon accelerate freely to the prescribed velocity and then move constantly with that speed. The root-mean-square error (*RMSE*) of the relative difference of the standard deviations between data and simulation is applied to measure the performance:

$$RMSE_{\sigma} = \sqrt{\frac{1}{24}\sum_{n=2}^{25}\left(\frac{\sigma_{v,n}^{\text{simu}} - \sigma_{v,n}^{\text{experi}}}{\sigma_{v,n}^{\text{experi}}}\right)^2} \tag{7}$$

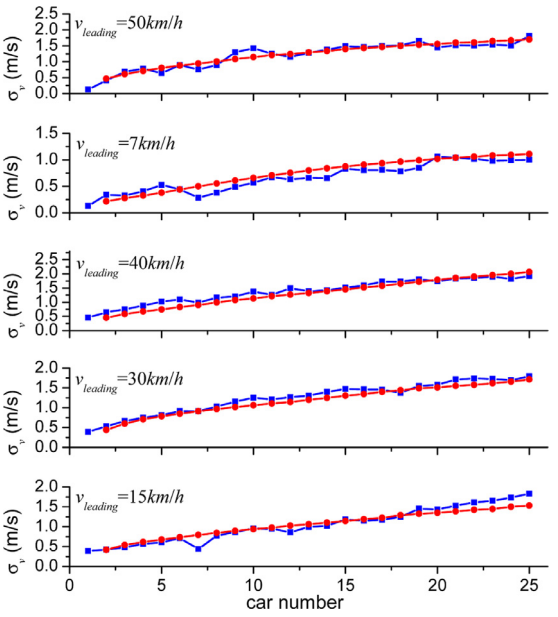

Fig. 10. Comparison of the simulation results (symbol solid red lines) and experiment results (symbol solid blue lines) of the standard deviation of the speed of the cars. The car number 1 is the leading car. (For interpretation of the references to colour in this figure legend, the reader is referred to the web version of this article.)

Table 4
The calibration and validation $RMSE_\sigma$ of the car following experiments.

Model		Calibration error		Validation error		
TSM	$v_{leading}$ (km/h)	50	7	40	30	15
	$RMSE_s$	0.11	0.25	0.13	0.09	0.19
	Average $RMSE_s$	0.18			0.14	
Two-State model	$v_{leading}$ (km/h)	50	7	40	30	15
	$RMSE_s$	0.21	0.31	0.32	0.26	0.29
	Average $RMSE_s$	0.26			0.29	

where n is the vehicle number, $\sigma_{v,n}^{simu}$ ($\sigma_{v,n}^{experi}$) represents the standard deviation of vehicle n in the stationary state in the simulation (experiments) . The standard deviation of the speed of each car in the simulation is calculated by

$$\sigma_{v,n} = \sqrt{\frac{\sum_{t=1}^{T_s} (v_n(t) - \overline{v_n})^2 \times L_{cell}^2}{T_s - 1}} \tag{8}$$

where $v_n(t)$ is the speed of vehicle n at time t (unit: L_{cell}/s), T_s is the time interval of the stationary state, $\overline{v_n}$ is the mean speed of vehicle n with the unit: L_{cell}/s and $L_{cell} = 0.5$ m. During the calibration, the objective is to minimize the average $RMSE_\sigma$ of the two runs with $v_{leading} = 50$ and 7 km/h. The calibration results are shown in Table 4, in which only p_b changes from 0.52 to 0.4, other parameters are the same as that in Table 3. Moreover, the calibration results of Two-State model are also given in Table 4, where L_{cell}, p_a, p_b, v_{max}, g_{safety} changes from 7.5, 0.95, 0.55, 5, 1, 2 to 0.5, 0.35, 0.3, 60, 20, respectively. Other parameters of Two-State model are the same as that in Table 1. It can be shown that the performance of TSM are much better than that of Two-State model.

It should be noted that the simulated variance ${\sigma_v}^2$ contains two components: (i) the true standard deviation ${\sigma_{dyna}}^2$ caused by the model dynamics; (ii) the standard deviation ${\sigma_{discr}}^2$ of the discretization error caused by the finite speed step $\Delta v = 1L_{cell}/s = 0.5$ m/s due to the discrete nature of cellular automaton. Since we can assume (without loss of generality) that the discretization error is unbiased, the difference between the "true" continuous speed and the discretized model is uniformly distributed with the ranges $[-\Delta v/2, \Delta v/2]$ resulting in a discretization error deviation:

$${\sigma_{discr}}^2 = \frac{\Delta v^2}{12} \approx 0.02 \tag{9}$$

It is plausible to assume that both stochastic terms are uncorrelated, so we have

$${\sigma_v}^2 = {\sigma_{discr}}^2 + {\sigma_{dyna}}^2 \tag{10}$$

Since ${\sigma_{discr}}^2$ is very small, the discretization error can be neglected.

Table 5
Calibration (07. April 2005) and validation errors (other days).

Model	07 Apr	08 Apr	11 Apr	12 Apr	13 Apr	14 Apr
TSM	0.19	0.18	0.16	0.15	0.15	0.20
Two-State model	0.18	0.18	0.16	0.16	0.16	0.29
BLM	0.38	0.50	0.34	0.32	0.34	0.47
KKW model	0.22	0.28	0.19	0.22	0.20	0.48

The calibration errors and validation errors are given in Table 4, both of which are small. While the fact that the validation error is even smaller than the calibration error is a contingency of this specific experiment, it generally indicates the capability of the TSM in predicting the observed growth of the disturbances along the platoon, see Fig. 10. Fig. 11 shows that the formation and evolution of the simulated oscillations (right panels) look very similar to that of Jiang's experimental data (left panels).

Furthermore, we compare the speed profile of different following vehicles in Jiang's experiments with the predictions of TSM. Since the TSM is a stochastic model, the probability distribution of the following vehicles was estimated by repeated simulations of the lead vehicle problems (LVPs, Laval et al., 2014). For a LVP, the leading vehicle is asked to move according to the experimental data,[3] while the following vehicle is modeled by the TSM. Fig. 12 presents several examples of experimental (red lines) and simulated velocity profiles of the following vehicles. The shaded areas are the simulated velocity profiles with 90%-probability band. One can see that the experimental profiles almost fall into the 90%-probability bands, which means that the movements of the following vehicles can be predicted by TSM. In order to determine the 90%-probability band, we have simulated the same situation 100 times with different random seeds for the pseudo-random number generator and determined, for each time step, the 5*th* and 95*th* percentile of the speed as the lower and upper bound of the 90%-probability bands.

4.2. Calibration and validation by detector data

We further test the performance of TSM by using the empirical data sets presented by NGSIM (2006), which are from double-loop detectors between Powell Street and Gilman Avenue on the five-lane Interstate 80 (I-80) in Emeryville, California (see Fig. 13). The method of Brockfeld et al. (2005) and Wagner (2010) is applied to calibrate and validate the TSM. The data sets from Detectors 6 and 4 offer the inflow and outflow boundary conditions while Detector 5 measures the performance of the models by comparing the simulated speed time series with the real data.

The data from the five-lane road are averaged to effectively single lane data (see details in Brockfeld et al. (2005)). Models will be calibrated with the data of Thursday, 07 April 2005 and then validated with the data of other five days. Again, the *RMSE* of the relative deviations will be applied as the objective function:

$$RMSE = \sqrt{\frac{1}{N}\sum_i \left(\frac{v^{5i}_{\text{simu}} - v^{5i}_{\text{ave}}}{v^{5i}_{\text{ave}}}\right)^2} \tag{11}$$

where v^{5i}_{simu} is the ith speed value of the simulation data at detector 5; v^{5i}_{ave} is the ith lane-average speed value of the empirical data at Detector 5; N is the number of the data points. Moreover, the original Two-state model, the Brake Light Model (BLM, which has been used by Hafstein et al. (2004) to simulate traffic flow on the autobahn network in North Rhine-Westphalia) and the KKW model have been calibrated and validated to make comparison with TSM.

The calibration and validation results are given in Table 5 and Fig. 14, which show that 1) although the TSM calibration error is almost the same as that of the Two-State model, the validation results are slightly better than Two-State model, especially on 14 Apr.; 2) Compared with the BLM and KKW models, both the calibration and validation errors of the TSM are much more smaller.

5. Conclusion

Traffic flow models play a significant role in traffic micro-simulations and models that can reproduce all observed traffic flow phenomena are most useful in advancing traffic flow theory. In a recent paper, Tian et al. (2015) have proposed the Two-state cellular automaton model based on the assumption that the space gap between two vehicles will oscillate around the (speed dependent) desired value rather than maintain this value in the deterministic limit in congested traffic flow. Although the Two-state model has successfully simulated the spatiotemporal patterns of traffic flow, it is not able to quantitatively replicate the important property that the standard deviation of the speed of a car is a concave function of its position number in a platoon.

Based on the Two-state model, this paper proposes the Two-state Safe-speed model (TSM) by introducing the safe speed and the logistic function of the randomization probability. Simulations show that the TSM can reproduce well all identified

[3] In the simulation, the speed of the leading car is set as $[v_l/3.6/L_{\text{cell}}]$.

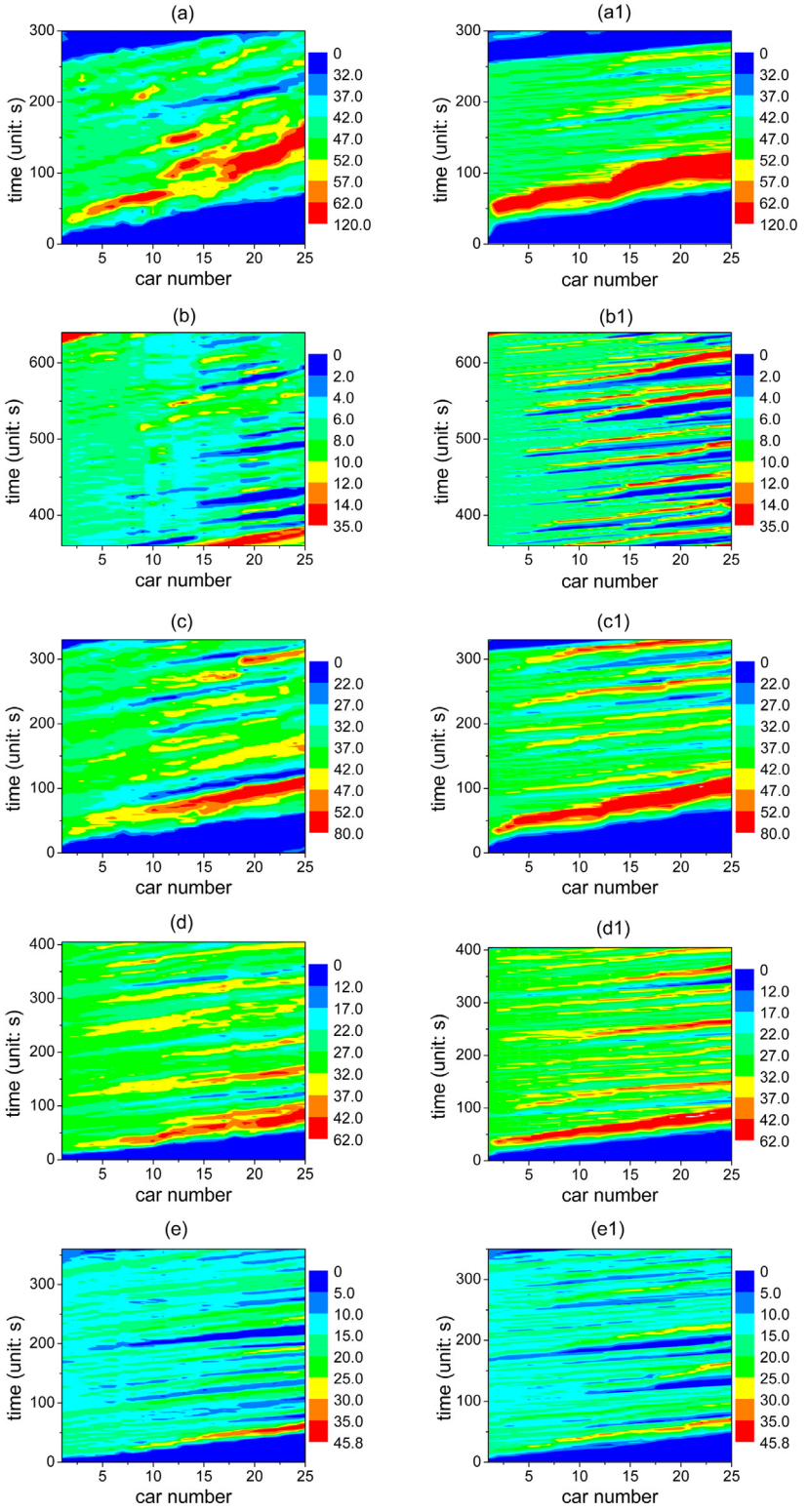

Fig. 11. The spatiotemporal patterns of the platoon traffic. The car speed is shown with different colors (unit: *km*/*h*) as function of time and car number. The left and right Panels show the experimental results and the simulation results of TSM. In (a, a1) - (e, e1), the leading vehicle of the platoon is required to move with $v_{leading} = 50$, 7, 40, 30, 15 km/h, respectively. In the simulation, the speed of the leading car of the platoon is set as $[v_{leading}/3.6/L_{cell}]$. The color bar indicates speed. (For interpretation of the references to colour in this figure legend, the reader is referred to the web version of this article.)

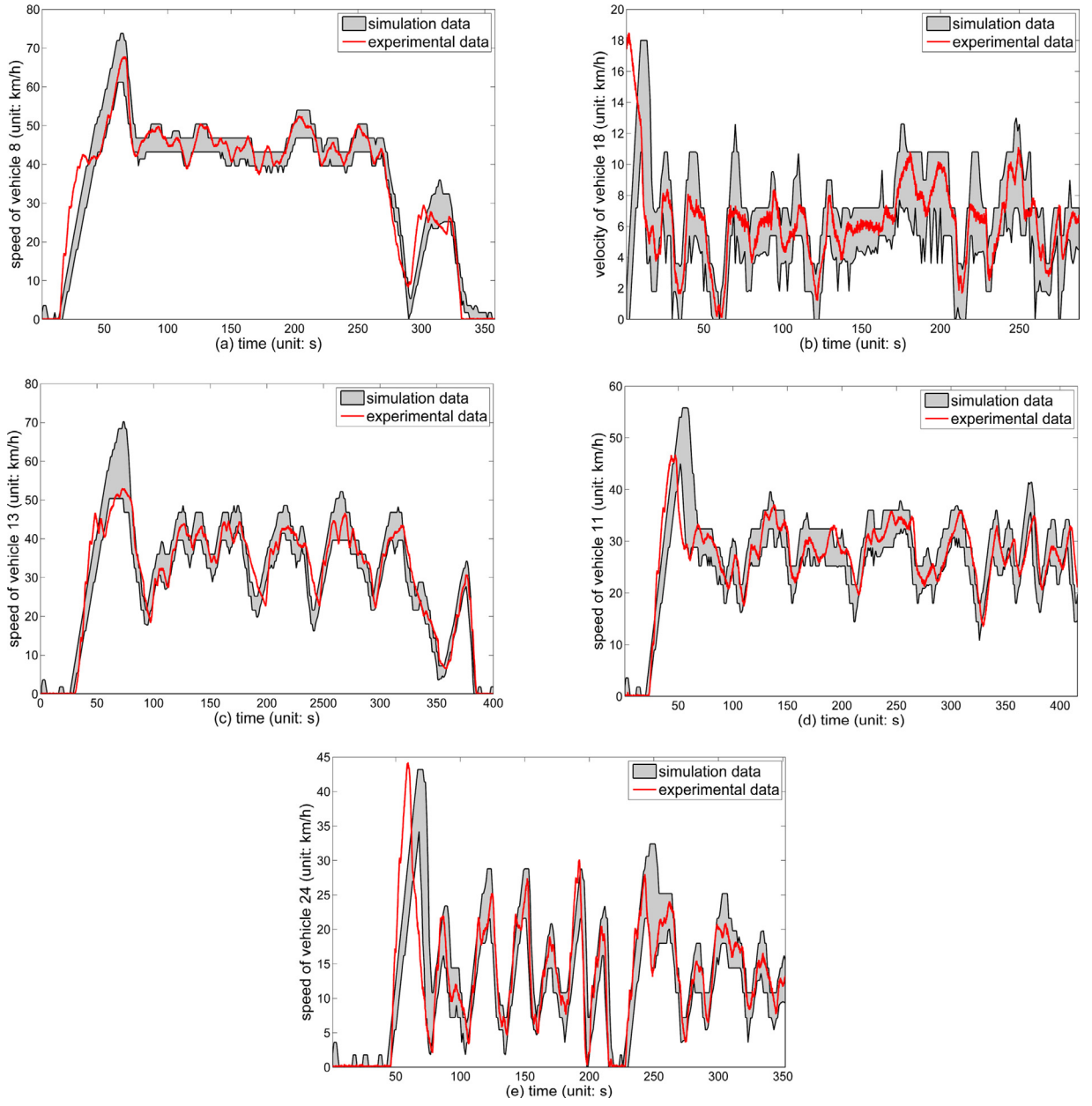

Fig. 12. Car following investigations. The red lines are the experimental velocity profiles of different following vehicles taken from Jiang's experiments. The shaded areas are the simulated velocity profiles with 90%-probability band. In (a)–(e), the leading vehicle of the platoon moves with $v_{leading} = 50$, 7, 40, 30, 15 km/h respectively. In the simulation, the speed of the leading car is set as $[v_l/3.6/L_{cell}]$. (For interpretation of the references to colour in this figure legend, the reader is referred to the web version of this article.)

phenomena. Specifically, simulations on a closed circular road show that TSM is able to depict the metastable state, free flow, synchronized flow, and jams as well as the transitions between these three phases. Simulations on an open road with an on-ramp demonstrate that the spatiotemporal patterns of traffic flow can be reproduced as well. Calibration and validation results show that TSM can simulate the concave growth pattern of traffic oscillations and the empirical time series of traffic speed.

Now following questions arises naturally: do there exist other traffic flow models that can simultaneously describe all known empirical and experimental features of traffic flow? Since traditional two-phase models such as the GMs, Gipps' Model, OVM, FVDM and IDM, fail to reproduce the growth pattern of the standard deviation of speed, we refer to the three-phase traffic models. We have examined the KKW model, the model of Lee, the MCD model, the model of Gao, and the 2D-IDM. Unfortunately, none of them could perform as well as the TSM. Specifically, the 2D-IDM fails to simulate the

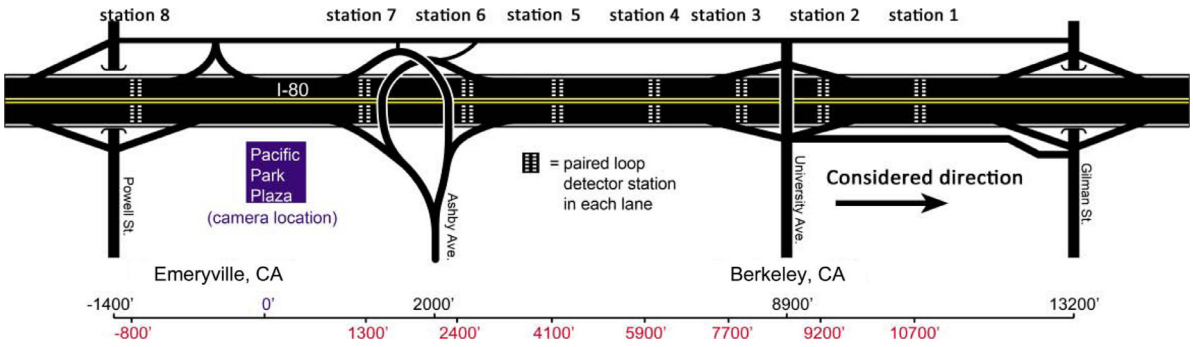

Fig. 13. Sketch of I-80 near Berkeley.

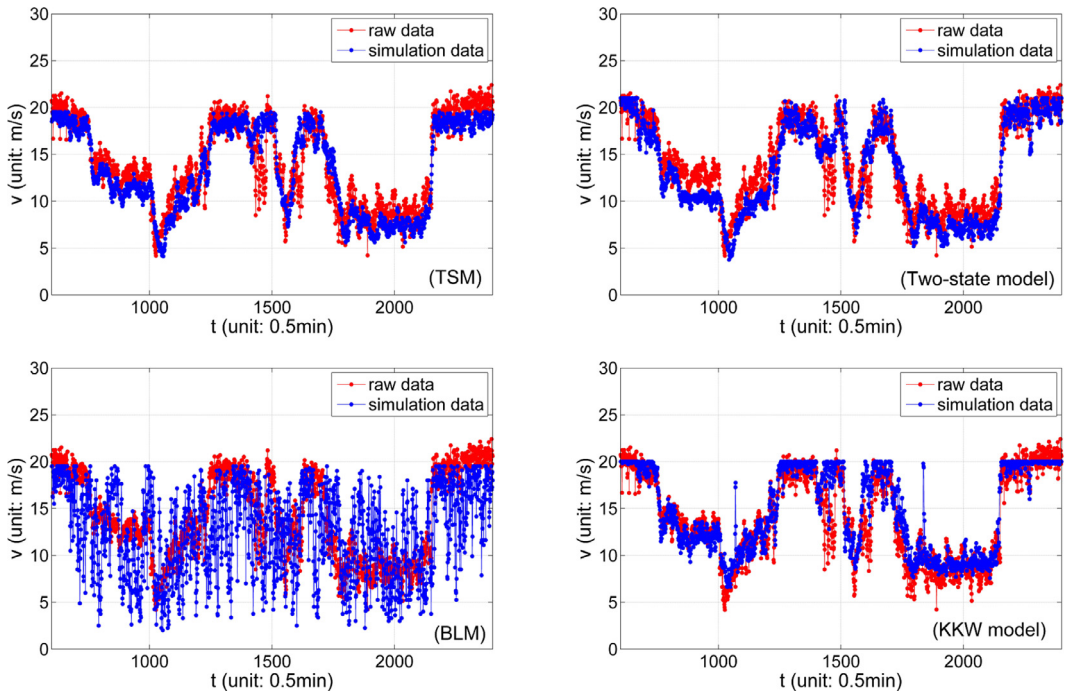

Fig. 14. Time series of speed at Station 5 on 07 Apr 2005.

synchronized traffic flow and the first order transition from free flow to synchronized flow; others cannot quantitatively simulate the concave growth pattern of speed oscillations.

However, although the cell length is set to 0.5 m, the TSM is still coarse-grained compared to car-following models which are continuous in both time and space. Therefore, efforts are needed to establish well-performing car-following models. On the other hand, due to the small cell size, it is worthwhile to compare TSM with some sort of generalization of the discrete version of the stochastic car following models, such as the model proposed by Laval et al (2014), where the acceleration is taken as a Brownian motion.

Acknowledgements

JFT was supported by the National Natural Science Foundation of China (Grant No. 71401120). RJ was supported by the Natural Science Foundation of China (Grant Nos. 11422221, 71371175, 71631002 and 71621001). SFM was supported by the National Natural Science Foundation of China (Grant No. 71431005 and 71671123).

References

Ahn, S., Cassidy, M.J., 2007. Freeway traffic oscillations and vehicle lane-change maneuvers. Transportation and Traffic Theory 2007 Papers Selected for Presentation at ISTTT17.

Aghabayk, K., Forouzideh, N., Young, W., 2013. Exploring a local linear model tree approach to car-following. Comput.-Aided Civil Infrastruct. Eng. 28 (8), 581–593.

Bando, M., Hasebe, K., Nakayama, A., Shibata, A., Sugiyama, Y., 1995. Dynamical model of traffic congestion and numerical simulation. Phys. Rev. E 51 (2), 1035.
Bertini, R.L., Monica, T.L., 2005. Empirical study of traffic features at a freeway lane drop. J. Transp. Eng. 131 (6), 397–407.
Brackstone, M., McDonald, M., 1999. Car-following: a historical review. Transp. Res. Part F 2 (4), 181–196.
Brockfeld, E., Kühne, R.D., Wagner, P., 2005. Calibration and validation of microscopic models of traffic flow. Transportation Research Record: Journal of the Transportation Research Board 1934 (1), 179–187.
Chandler, R.E., Herman, R., Montroll, E.W., 1958. Traffic dynamics: studies in car following. Oper. Res. 6 (2), 165–184.
Chen, D., Laval, J.A., Ahn, S., Zheng, Z., 2012a. Microscopic traffic hysteresis in traffic oscillations: a behavioral perspective. Transp. Res. Part B 46, 1440–1453.
Chen, D., Laval, J.A., Zheng, Z., Ahn, S., 2012b. A behavioral car-following model that captures traffic oscillations. Transp. Res. Part B 46, 744–761.
Chowdhury, D., Santen, L., Schadschneider, A., 2000. Statistical physics of vehicular traffic and some related systems. Phys. Rep. 329 (4), 199–329.
Coifman, B., 1997. Time space diagrams for thirteen shock waves. California Partners for Advanced Transit and Highways (PATH).
Gao, K., Jiang, R., Hu, S.-X., Wang, B.-H., Wu, Q.-S., 2007. Cellular-automaton model with velocity adaptation in the framework of Kerner's three-phase traffic theory. Phys. Rev. E 76 (2), 026105.
Gao, K., Jiang, R., Wang, B.-H., Wu, Q.-S., 2009. Discontinuous transition from free flow to synchronized flow induced by short-range interaction between vehicles in a three-phase traffic flow model. Physica A 388 (15), 3233–3243.
Edie, L.C., 1961. Car-following and steady-state theory for noncongested traffic. Oper. Res. 9 (1), 66–76.
Gazis, D.C., Herman, R., Rothery, R.W., 1961. Nonlinear follow-the-leader models of traffic flow. Oper. Res. 9 (4), 545–567.
Gipps, P.G., 1981. A behavioural car-following model for computer simulation. Transp. Res. Part B 15 (2), 105–111.
Hafstein, S., Chrobok, R., Pottmeier, A., Schreckenberg, M., Mazur, F.C., 2004. A high-resolution cellular automata traffic simulation model with application in a freeway traffic information system. Comput. Aided Civil Infrastruct. Eng. 19 (5), 338–350.
Helbing, D., 2001. Traffic and related self-driven many-particle systems. Rev. Modern Phys. 73 (4), 1067.
He, Z., Zheng, L., Guan, W., 2015. A simple nonparametric car-following model driven by field data. Transp. Res. Part B 80, 185–201.
Jiang, R., Wu, Q., Zhu, Z., 2001. Full velocity difference model for a car-following theory. Phys. Rev. E 64 (1), 017101.
Jiang, R., Wu, Q.-S., 2003. Cellular automata models for synchronized traffic flow. J. Phys. A 36 (2), 381.
Jiang, R., Wu, Q., 2005. First order phase transition from free flow to synchronized flow in a cellular automata model. Eur. Phys. J. B-Condensed Matter Complex Syst. 46 (4), 581–584.
Jiang, R., Hu, M.B., Zhang, H.M., Gao, Z.Y., Jia, B., Wu, Q.-S., Wang, B., Yang, M., 2014. Traffic experiment reveals the nature of car-following. PloS one 9 (4), e94351.
Jiang, R., Hu, M.B., Zhang, H.M., Gao, Z.Y., Jia, B., Wu, Q.S., 2015. On some experimental features of car-following behavior and how to model them. Transp. Res. Part B 80, 338–354.
Jin, C.J., Wang, W., Jiang, R., Zhang, H.M., Wang, H., Hu, M.B., 2015. Understanding the structure of hyper-congested traffic from empirical and experimental evidences. Transp. Res. Part C 60, 324–338.
Kerner, B.S., 1998. Experimental features of self-organization in traffic flow. Phys. Rev. Lett. 81 (17), 3797.
Kerner, B.S., Klenov, S.L., Wolf, D.E., 2002. Cellular automata approach to three-phase traffic theory. J. Phys. A 35 (47), 9971.
Kerner, B.S., 2004. The physics of traffic: empirical freeway pattern features, engineering applications, and theory. Springer Science & Business Media.
Kerner, B.S., 2009. Introduction to modern traffic flow theory and control: the long road to three-phase traffic theory. Springer Science & Business Media.
Kerner, B.S., Klenov, S.L., Schreckenberg, M., 2011. Simple cellular automaton model for traffic breakdown, highway capacity, and synchronized flow. Phys. Rev. E 84 (4), 046110.
Kerner, B.S., 2013. Criticism of generally accepted fundamentals and methodologies of traffic and transportation theory: A brief review. Phys. A 392 (21), 5261–5282.
Kerner, B.S., 2016. Failure of classical traffic flow theories: Stochastic highway capacity and automatic driving. Phys. A doi:10.1016/j.physa.2016.01.034.
Kesting, A., Treiber, M., 2008. How reaction time, update time, and adaptation time influence the stability of traffic flow. Comput. Aided Civil Infrastruct. Eng. 23 (2), 125–137.
Knospe, W., Santen, L., Schadschneider, A., Schreckenberg, M., 2000. Towards a realistic microscopic description of highway traffic. J. Phys. A 33 (48), L477.
Newell, F.G., 2002. A simplified car-following theory: a lower order model. Transp. Res. Part B 36 (3), 195–205.
Laval, J.A., Daganzo, C.F., 2006. Lane-changing in traffic streams. Transp. Res. Part B 40 (3), 251–264.
Laval, J.A., Leclercq, L., 2010. A mechanism to describe the formation and propagation of stop-and-go waves in congested freeway traffic. Philosophical Trans. Royal Soc. A 368, 4519–4541.
Laval, J.A., Toth, C.S., Zhou, Y., 2014. A parsimonious model for the formation of oscillations in car-following models. Transp. Res. Part B 70, 228–238.
Lee, H.K., Barlovic, R., Schreckenberg, M., Kim, D., 2004. Mechanical restriction versus human overreaction triggering congested traffic states. Phys. Rev. Lett. 92 (23), 238702.
Lighthill, M.J., Whitham, G.B., 1955. On kinematic waves. II. A theory of traffic flow on long crowded roads. Proc. Royal Soc. London A: Mathematical, Physical and Engineering Sciences. The Royal Society 229 (1178), 317–345.
Maerivoet, S., De Moor, B., 2005. Cellular automata models of road traffic. Phys. Reports 419 (1), 1–64.
Nagatani, T., 2002. The physics of traffic jams. Reports Progress Phys. 65 (9), 1331.
Nagel, K., Schreckenberg, M., 1992. A cellular automaton model for freeway traffic. Journal de physique I 2 (12), 2221–2229.
Nakayama, A., Fukui, M., Kikuchi, M., Hasebe, K., Nishinari, K., Sugiyama, Y., et al., 2009. Metastability in the formation of an experimental traffic jam. New J. Phys. 11 (8), 083025.
NGSIM, 2006 Next generation simulation. http://ngsim.fhwa.dot.gov/
Papageorgiou, M., 1998. Some remarks on macroscopic traffic flow modelling. Transp. Res. Part A 32 (5), 323–329.
Rakha, H., Crowther, B., 2003. Comparison and calibration of FRESIM and INTEGRATION steady-state car-following behavior. Transp. Res. Part A 37 (1), 1–27.
Ranjitkar, P., Nakatsuji, T., Azuta, Y., Gurusinghe, G., 2003. Stability analysis based on instantaneous driving behavior using car-following data. Transp. Res. Record 1852 (1), 140–151.
Saifuzzaman, M., Zheng, Z., 2014. Incorporating human-factors in car-following models: a review of recent developments and research needs. Transp. Res. Part C 48, 379–403.
Shott, M.J., 2011. Traffic Oscillations Due To Topology and Route Choice in Elemental Freeway Networks. University of California Ph. D. thesis.
Sugiyama, Y., Fukui, M., Kikuchi, M., Hasebe, K., Nakayama, A., Nishinari, K., Tadaki, S., Yukawa, S., 2008. Traffic jams without bottlenecks—experimental evidence for the physical mechanism of the formation of a jam. New J. Phys. 10 (3), 033001.
Tadaki, S., Kikuchi, M., Fukui, M., Nakayama, A., Nishinari, K., Shibata, A., Sugiyama, Y., Yosida, T., Yukawa, S., 2013. Phase transition in traffic jam experiment on a circuit. New J. Phys. 15 (10), 103034.
Tian, J.F., Jia, N., Zhu, N., Jia, B., Yuan, Z.Z., 2014. Brake light cellular automaton model with advanced randomization for traffic breakdown. Transp. Res. Part C 44, 282–298.
Tian, J.F., Treiber, M., Ma, S.F., Jia, B., Zhang, W.Y., 2015. Microscopic driving theory with oscillatory congested states: model and empirical verification. Transp. Res. Part B 71, 138–157.
Tian, J., Jiang, R., Jia, B., Hu, M.B., Zhang, W., Jia, N., Ma, S., 2016a. Empirical analysis and simulation of the evolution concavity of traffic oscillations. Transp. Res. Part B 93, 338–354.
Tian, J., Jia, B., Ma, S., Zhu, C., Jiang, R., Ding, Y., 2016b. Cellular Automaton Model with Dynamical 2D Speed-Gap Relation. Transp. Sci.. http://dx.doi.org/10.1287/trsc.2015.0667.
Treiber, M., Hennecke, A., Helbing, D., 2000. Congested traffic states in empirical observations and microscopic simulations. Phys. Rev. E 62 (2), 1805.

Treiber, M., Kesting, A., Helbing, D., 2010. Three-phase traffic theory and two-phase models with a fundamental diagram in the light of empirical stylized facts. Transp. Res. Part B 44 (8), 983–1000.
Treiber, M., Kesting, A., 2013. Traffic flow dynamics. Traffic Flow Dynamics: Data, Models and Simulation. Springer-Verlag, Berlin, Heidelberg.
Treiterer, J., Myers, J., 1974. The hysteresis phenomenon in traffic flow. Transp. Traffic Theory 6, 13–38.
Wagner, P., 2006. How human drivers control their vehicle. Eur. Phys. J. B 52 (3), 427–431.
Wagner, P., 2010. Fluid-dynamical and microscopic description of traffic flow: a data-driven comparison. Philosophical Trans. Royal Soc. London. Series B, Biological sciences 368 (1928), 4481–4495.
Wagner, P., 2012. Analyzing fluctuations in car-following. Transp. Res. Part B 46 (10), 1384–1392.
Wong, G.C.K., Wong, S.C., 2002. A multi-class traffic flow model–an extension of LWR model with heterogeneous drivers. Transp. Res. Part A 36 (9), 827–841.
Zheng, Z., 2014. Recent developments and research needs in modeling lane changing. Transp. Res. Part B 60, 16–32.
Zheng, Z.D., Ahn, S., Chen, D.J., Laval, J., 2011. Applications of wavelet transform for analysis of freeway traffic: Bottlenecks, transient traffic, and traffic oscillations. Transp. Res. Part B 45 (2), 372–384.